UNCLASSIFIED

AD NUMBER

AD854724

NEW LIMITATION CHANGE

TO

Approved for public release, distribution unlimited

FROM

Distribution authorized to U.S. Gov't. agencies and their contractors; Administrative/Operational Use; May 1969. Other requests shall be referred to Commanding Officer, US Army Aberdeen Research & Development Center, Aberdeen Proving Ground, MD.

AUTHORITY

DoDD 5230.24

THIS PAGE IS UNCLASSIFIED

BRL MR 1981

AD854724

BRL

AD

MEMORANDUM REPORT NO. 1981

DRAG AND STABILITY PROPERTIES OF THE XM144 FLECHETTE WITH VARIOUS HEAD SHAPES

by

L. C. MacAllister

May 1969

U.S. ARMY ABERDEEN RESEARCH AND DEVELOPMENT CENTER
BALLISTIC RESEARCH LABORATORIES
ABERDEEN PROVING GROUND, MARYLAND

42

B A L L I S T I C   R E S E A R C H   L A B O R A T O R I E S

MEMORANDUM REPORT NO. 1981

MAY 1969

DRAG AND STABILITY PROPERTIES OF THE XM144 FLECHETTE WITH VARIOUS HEAD SHAPES

L. C. MacAllister

Exterior Ballistics Laboratory

RDT&E Project No. 1T262301A201

A B E R D E E N   P R O V I N G   G R O U N D,   M A R Y L A N D

B A L L I S T I C R E S E A R C H L A B O R A T O R I E S

MEMORANDUM REPORT NO. 1981

LCMacAllister/pp
Aberdeen Proving Ground, Md.
May 1969

DRAG AND STABILITY PROPERTIES OF THE XM144 FLECHETTE WITH VARIOUS HEAD SHAPES

ABSTRACT

The drag and stability properties of a family of flechettes with conical heads are presented; cone semi-angles varied from 5 to 90 degrees. The data cover a range from Mach 2 to Mach 4 and were determined from free flight spark range tests. Limited results on a spike-nosed configuration are also given.

TABLE OF CONTENTS

	Page
ABSTRACT	3
LIST OF SYMBOLS	7
INTRODUCTION	9
TEST OUTLINE	10
RESULTS	12
1. Test Family	17
Drag Coefficient	17
Static Moment	20
Normal Force Slope	24
Damping Moment Coefficient	26
2. Component Properties	26
Drag	26
Static Moment	31
Normal Force Slope	32
3. Spike-Nosed Projectile	37
REFERENCES	42
DISTRIBUTION LIST	43

LIST OF SYMBOLS

C_D	Drag coefficient, $\dfrac{\text{Drag force}}{\frac{\rho V^2}{2} S}$
C_{N_α}	Normal force slope, $\dfrac{\text{Normal force}}{\frac{\rho V^2}{2} S\alpha}$
C_{M_α}	Static moment slope, $\dfrac{\text{Pitching moment}}{\frac{\rho V^2}{2} Sd\alpha}$
C_{M_q}	Pitch damping derivative, $\dfrac{\text{Pitching moment}}{\frac{\rho V^2}{2} Sd \frac{\delta d}{V}}$
$C_{M_{\dot\alpha}}$	Pitch damping derivative, $\dfrac{\text{Yawing moment}}{\frac{\rho V^2}{2} Sd \frac{\dot\alpha d}{V}}$
d	Body diameter
ℓ	Projectile length
W	Projectile weight
I_y	Transverse moment of inertia
S	Cross sectional area, $\frac{\pi d^2}{4}$
c.g.	Center of gravity from base
θ_s	Nose cone semi-angle
ρ	Air density
V	Projectile velocity
M	Mach number
α	Angle of attack
$\dot\alpha$	Rate of change of α
q	Pitch rate

INTRODUCTION

The conventional small flechette designed for use in a rifle system usually has a long conical or ogival head, a long cylindrical section, fins with a span of two to three calibers, and is of a single material. The long nose and the minimal fin size are usually dictated in order to maintain a low drag and, hence, a low retardation. This need, or desire, for a low drag configuration imposes some difficulties in the design of flechettes for other systems. Among these can be: desirable round length may be difficult to achieve with a high ℓ/d flechette of adequate weight, mechanical failure is more of a problem with a high ℓ/d body, and a homogeneous long projectile with minimal fins often has a small static stability margin, hence, a high sensitivity to initial launch disturbance. This latter problem has been recognized in the design of fin-stabilized anti-tank projectiles for many years and there have been two quite different solutions: low drag projectiles that are subcaliber and have a sabot that launches them consistently with very small yaw so that accuracy is preserved in spite of high sensitivity to launch disturbance, and projectiles with high drag noses which can be relatively compact, have adequate stability and low sensitivity to initial disturbance.

The testing of some fully blunted short flechettes in a multiple launch system demonstrated the higher accuracy expected compared with more conventional flechettes, and also the expected higher retardation. In order to provide information that would assist in evaluating intermediate designs, some free flight range tests were made using XM144 flechettes[1] with various conical head shapes having cone semi-angles from 5 to 90°. A few non-conical nose shapes were also tested.

The XM144 was selected as the basic component for modification because of its availability and because it is, for such a small projectile, very well made and has relatively thin, clean fins. These features would make the round-to-round data more consistent, which is quite desirable for a basic program, yet because of these features it also usually has a laminar boundary layer in flight and the flow in the area of the fins is relatively undisturbed. Some of the aerodynamic properties ascribed to the flechette as a whole and derived for the tail section in this report could well be different for a more crudely made vehicle.

TEST OUTLINE

The developmental XM144 flechette is made of steel, is 1.78mm in body diameter, has a fin span of about 5.33mm, and has a simple conical or a compound conical head. The projectiles for the present tests were fabricated from the parent models by remachining the head using a fixed length of 27.94mm from the base of the projectile to the shoulder of the conical head shape. Because of this restriction set by the basic projectile, the final projectiles used in this test varied in both weight and length as the head shape varied. The nominal dimensions of the projectiles tested are given in Figure 1 and the measured physical properties in Table I.

The projectiles were all launched from 7.62mm smoothbore tubes through the spark shadowgraphic Aerodynamics Range[2]. At the higher velocities, the Special Purpose Individual Weapon (SPIW) puller-sabot system was utilized while at the lower speeds a plastic-metal pusher sabot was used.

The basic test was conducted at Mach 4, but there was considerable velocity dispersion resulting in data at lower velocities as well. After this occurred and the major point

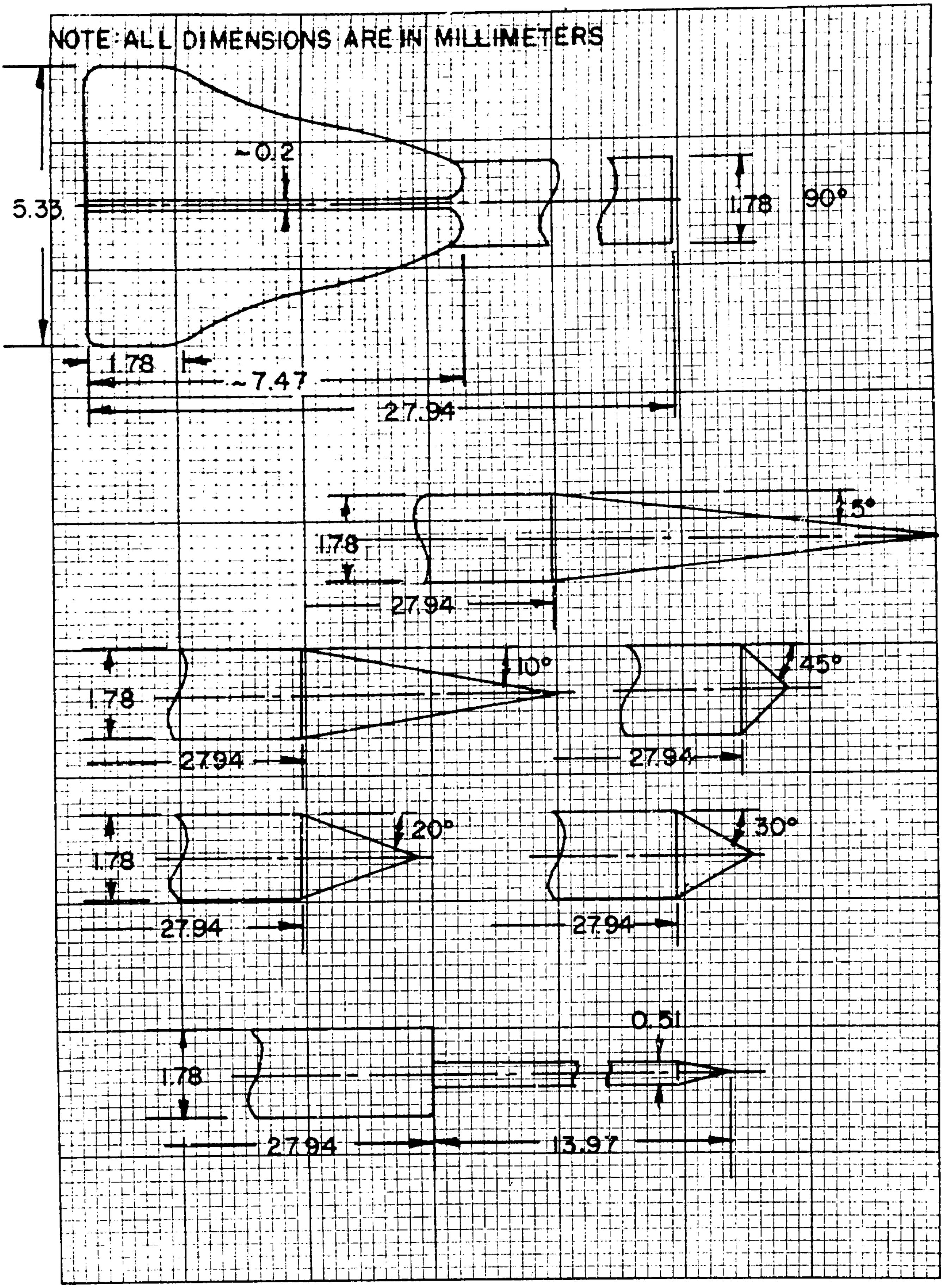

Figure 1. Projectile Configurations

was covered, the surplus models were deliberately launched at lower velocities to yield a semblance of a Mach number test between Mach 1.5 and 4 although the coverage below Mach 3 is sparse. Flight shadowgraphs of each type tested are given in Figures 2a-i.

Table I. Physical Properties of Modified XM144 Flechettes

Nose Type	Head Length (cal.)	Total Length (cal.)	Wt. (gram)	d (mm)	I_y ($gm\ cm^2$)	c.g. (cal. from base)	d_{fin} (mm)
Spike	7.87	23.5	.526	1.793	.406	9.06	5.309
90°	0	15.7	.4945	1.788	.297	8.46	5.283
45°	.49	16.2	.5029	1.783	.319	8.50	5.283
30°	.86	16.6	.5083	1.788	.320	8.63	5.283
20°	1.34	17.1	.5072	1.783	.322	8.74	5.283
15°	1.83	17.5	.5142	1.781	.338	8.84	5.283
10°	2.84	18.6	.5252	1.786	.359	9.06	5.283
5°	5.64	21.4	.5651	1.788	.444	9.54	5.283

RESULTS

The aerodynamic data collected consists primarily of drag and static moment coefficients, although some values of the normal force slope and the damping moment derivatives were also obtained. The range data were processed assuming that the projectile was symmetric,[3] although even well made flechettes have sufficient manufacturing asymmetries to develop measureable trim yaws and spin. The projectiles are so small that it is difficult to accurately determine the

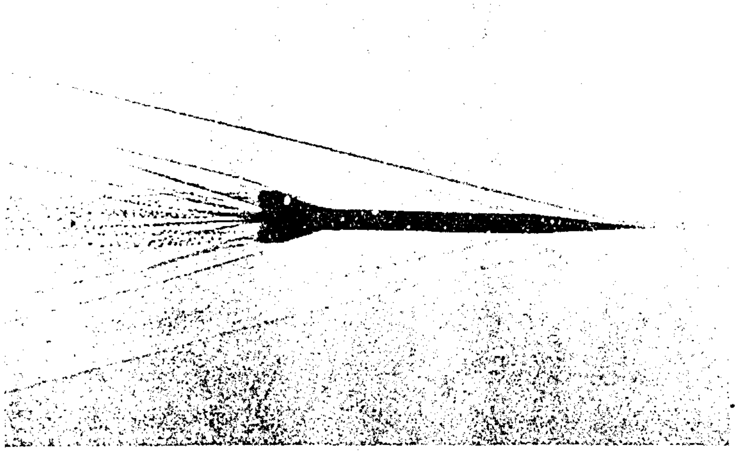

a. $\theta_s = 5^\circ$ $M = 4.2$

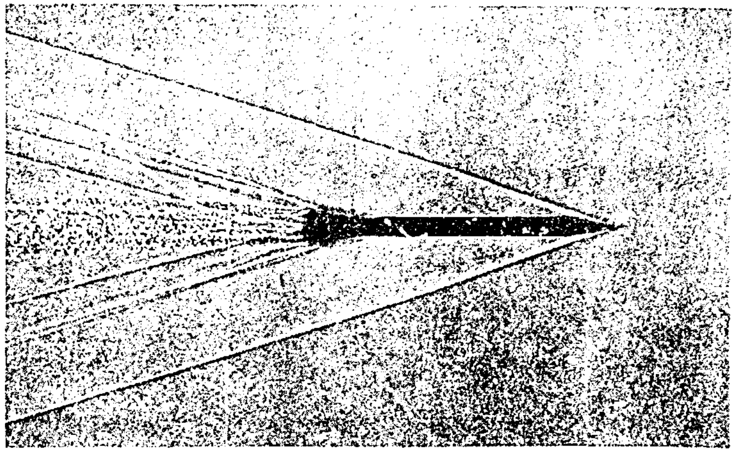

b. $\theta_s = 10^\circ$ $M = 3.6$

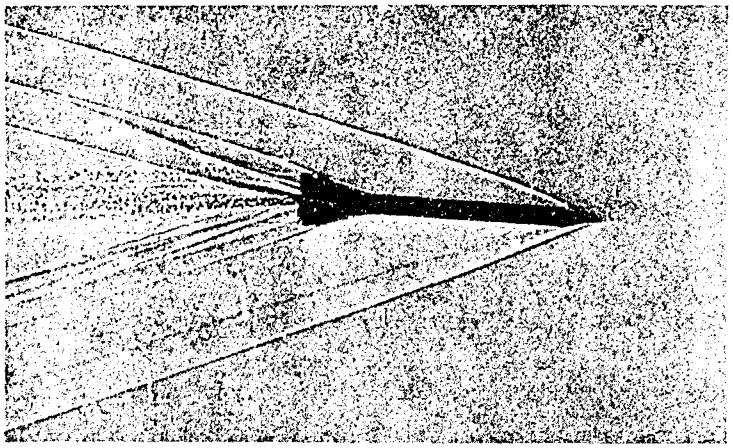

c. $\theta_s = 15^\circ$ $M = 3.5$

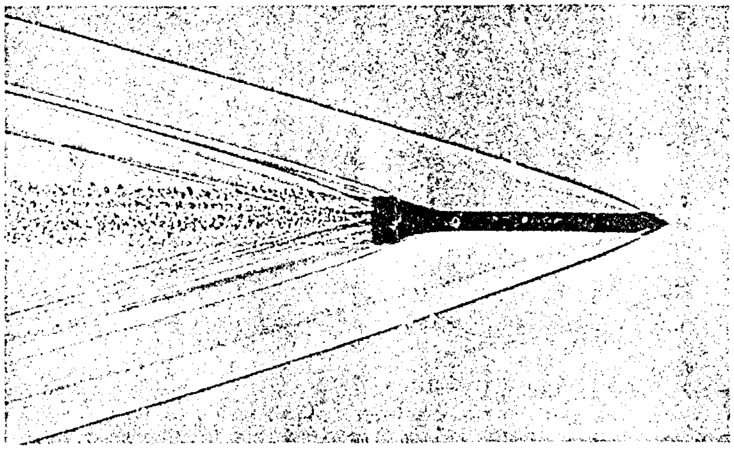

d. $\theta_s = 20^\circ$ $M = 3.7$

Figure 2. Shadowgraphs

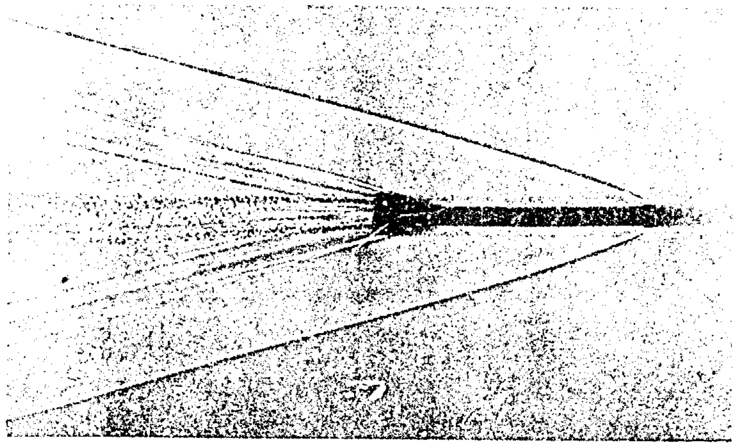

e. $\theta_s = 30^\circ$ $M = 4.1$

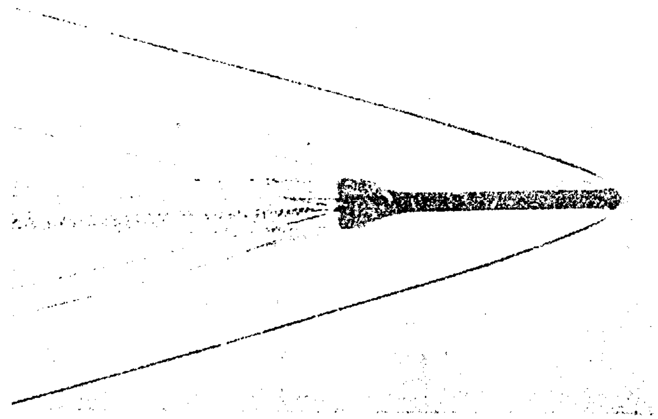

f. $\theta_s = 45^\circ$ $M = 4.0$

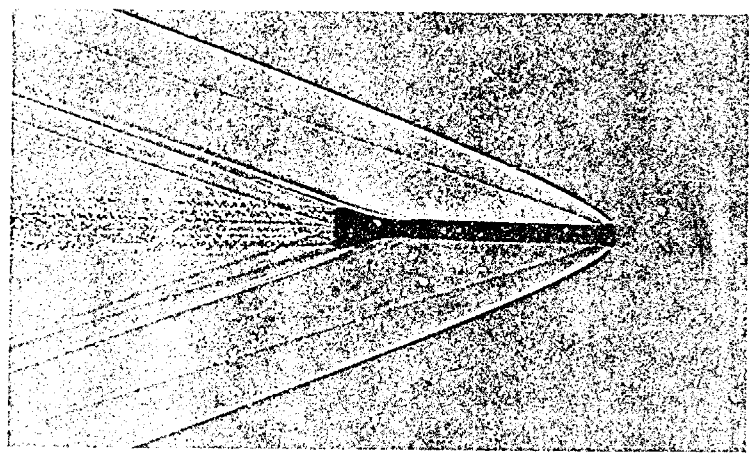

g. $\theta_s = 90^\circ$ $M = 3.0$

Figure 2. Shadowgraphs (Continued)

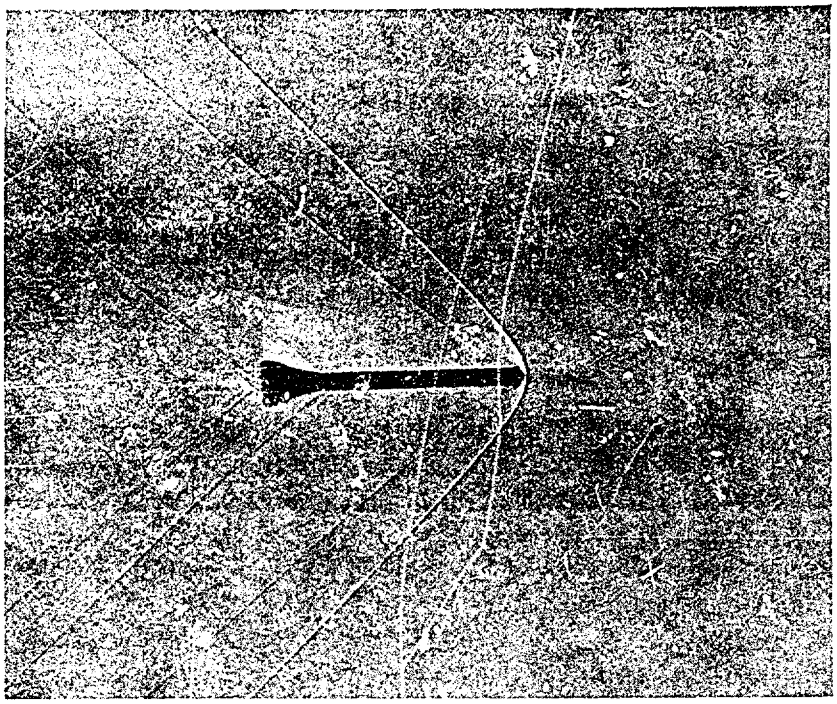

h. $\theta_s = 10^\circ$, $M = 1.4$ - Subsonic Fins

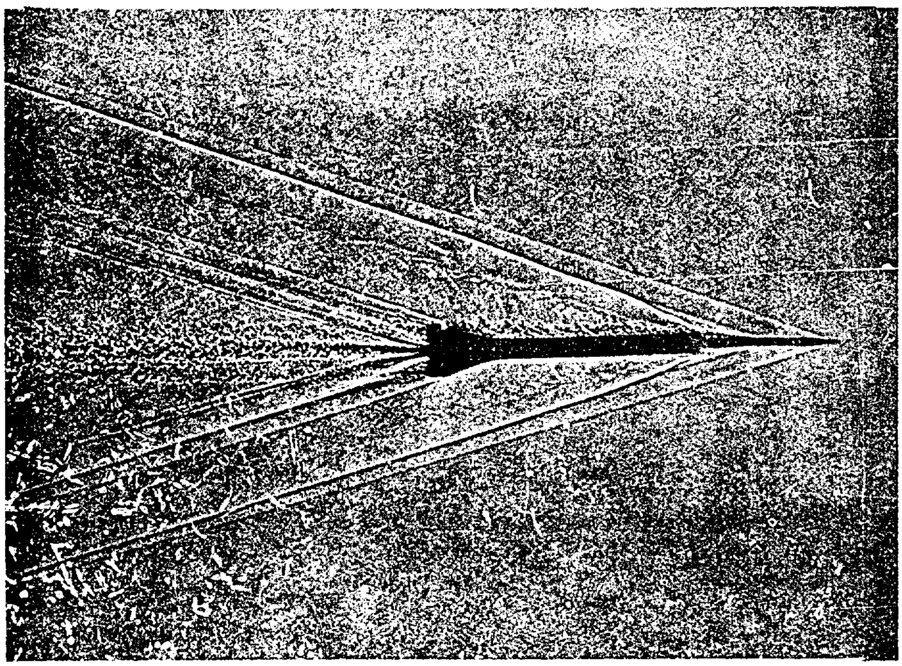

i. Spike-Nose $M = 3.5$

Figure 2. Shadowgraphs (Continued)

rolling motion and this determination is necessary if the asymmetric yawing motion is to be processed adequately. Because of this condition, there is a low percentage of C_{N_α} and $(C_{M_q} + C_{M_{\dot{\alpha}}})$ determinations.

The basic data independently establish the aerodynamic properties of the various configurations only at Mach 4. At the lower Mach numbers, it was necessary to devise a method to consider the data from several types together. The method selected was to compute the aerodynamic properties of the body alone using Van Dyke's second order theory[4] for the potential flow with a boundary layer thickness correction based on boundary layer computations of an insulated flat plate. This computation yields C_{D_o}, $C_{D_{\delta^2}}$, C_{N_α}, and CP_N, for the body. The validity limits permitted computations of the 5° and 10° θ_s cases at Mach 2, 3, and 4 but restricted the 15° θ_s case to less than Mach 3.5, the 20° θ_s case to Mach 2.5, and the 30° θ_s case to Mach 1.8. As a result, the desynthesis attempt could be made only on the first three cases initially. The subtraction of the body properties from the measured total properties yields the aerodynamic properties of the fin section which should be much more nearly the same than the total configuration properties. It should be noted, however, that the fin properties now include both the body-on-fin interference and any fin-on-body interference effects. This stripping process did seem to show that the tail section properties were invariant for the 5°, 10°, and 15° θ_s cases. The results were faired together and the process reversed to reconstruct curves for the whole configuration. Thus, the final data curves result both from direct and indirect inferences. The procedure inherently opened up the possibility of discussing the component properties as well as the total properties. The

component properties are interesting in that they permit the synthesis of flechette families other than the one tested; with the caution that the mutual interference between the body and tail may change if the bodies used are considerably different than those used in this test.

The process employed for the 5° to 15° θ_s cases seemed worthwhile to carry on for the other cases as at least a consistency check, but the lack of computations at the higher Mach numbers for the 20° and 30° θ_s conditions and at all Mach numbers for the remaining cases posed a problem. This was resolved for the conical head shapes by utilizing tabled values for the drag and normal force for cones, and using the previously determined skin friction and boundary layer corrections to C_{N_α} as approximations for these cases. Cruder approximations had to be used for the 90° θ_s and spike-nosed cases. The drag for the 90° nose was taken from the design curves of reference 5 (Vol. II), while the drag of the spike-nosed configuration and the normal force of both configurations were estimated from data on larger projectiles of similar head shapes. The estimates of the body contributions probably are decreasing in accuracy from the 5°-15° cases to the blunt cases.

The results for the test family are presented first and the component data follow. The results for the spike-nosed projectile are presented separately because it is not a logical parametric member of the family of configurations.

1. Test Family

Drag Coefficient. The drag coefficient data as determined from each individual test is given in Table II and the C_D is plotted in Figure 3 as a function of Mach number utilizing the test values adjusted to a zero yaw value where possible. The variation of C_D with yaw level

Table II. Aerodynamic Data

Round No.	θ_s (deg)	Mach No.	$\sqrt{\overline{\delta^2}}$ (deg)	C_D	$-C_{M_\alpha}$	$-(C_{M_q} + C_{M_{\dot{\alpha}}})$	C_{N_α}
1-7654	5	4.22	1.8	0.313	40.8	1260	10.4
7653	5	4.20	1.1	0.318	44.3	1150	
7675	5	3.45	1.0	0.329	55.5	--	
7688	5	2.60	1.0	0.483	74.4	1400	
7684	5	2.00	0.7	0.581	47.2	--	
1-7651	10	4.33	4.2	0.415	38.6	940	11.3
7665	10	4.26	1.6	0.339	35.5	600	11.4
7652	10	4.20	1.1	0.324	34.0	900	
7676	10	3.57	2.7	0.479	39.4	630	
7685	10	1.51	1.3	0.875	28.8	--	
1-7649	15	4.27	2.3	0.460	30.3	860	
7666	15	4.21	1.3	0.437	29.4	740	
7650	15	3.91	4.6	0.541	28.9	680	11.3
7674	15	3.50	8.1	0.581	37.3	1360	11.9
7687	15	2.42	2.1	0.692	75.1	1250	14.4
1-7647	20	4.37	4.0	0.639	27.8	640	10.2
7648	20	4.35	3.3	0.578	24.7	710	8.9
7672	20	3.70	1.7	0.707	40.2	--	
7686	20	2.59	0.4	0.729	65.5	--	
1-7646	30	4.27	2.4	0.832	28.9	590	11.4
7645	30	4.13	1.5	0.774	30.4	700	
7677	30	3.97	2.7	0.859	28.1	750	10.7
7683	30	3.46	1.0	0.890	36.9	--	
7689	30	2.32	1.7	1.139	76.3	1200	
1-7679	45	4.10	0.8	1.321	31.3	660	
7643	45	4.01	2.0	1.386	33.1	700	5.5
7644	45	3.96	1.5	1.369	33.7	570	
7681	45	3.30	2.5	1.410	46.5	840	10.2
7680	45	2.86	7.4	1.866	45.3	--	7.5
7692	45	1.49	5.6	1.838	13.6	1600	5.4
1-7642	90	4.24	2.7	1.757	37.8	480	6.4
7641	90	4.00	1.5	1.858			
7682	90	3.09	3.0	1.746	56.2	1090	
7671	90	2.96	2.8	1.642			
7693	90	2.43	2.0	1.612	73.8	610	8
7694	90	2.43	3.0	1.568	65.5	1300	
1-7664	Spike	4.08	2.0	0.540	24.7	--	Short spike
7697	"	3.44	1.4	0.564	50.1	930	8.2
7698	"	2.85	3.4	--	62.3	1220	14.1
7691	"	2.16	1.3	0.863	83.0	1500	
7690	"	2.10	2.1	0.945	86.4	1530	

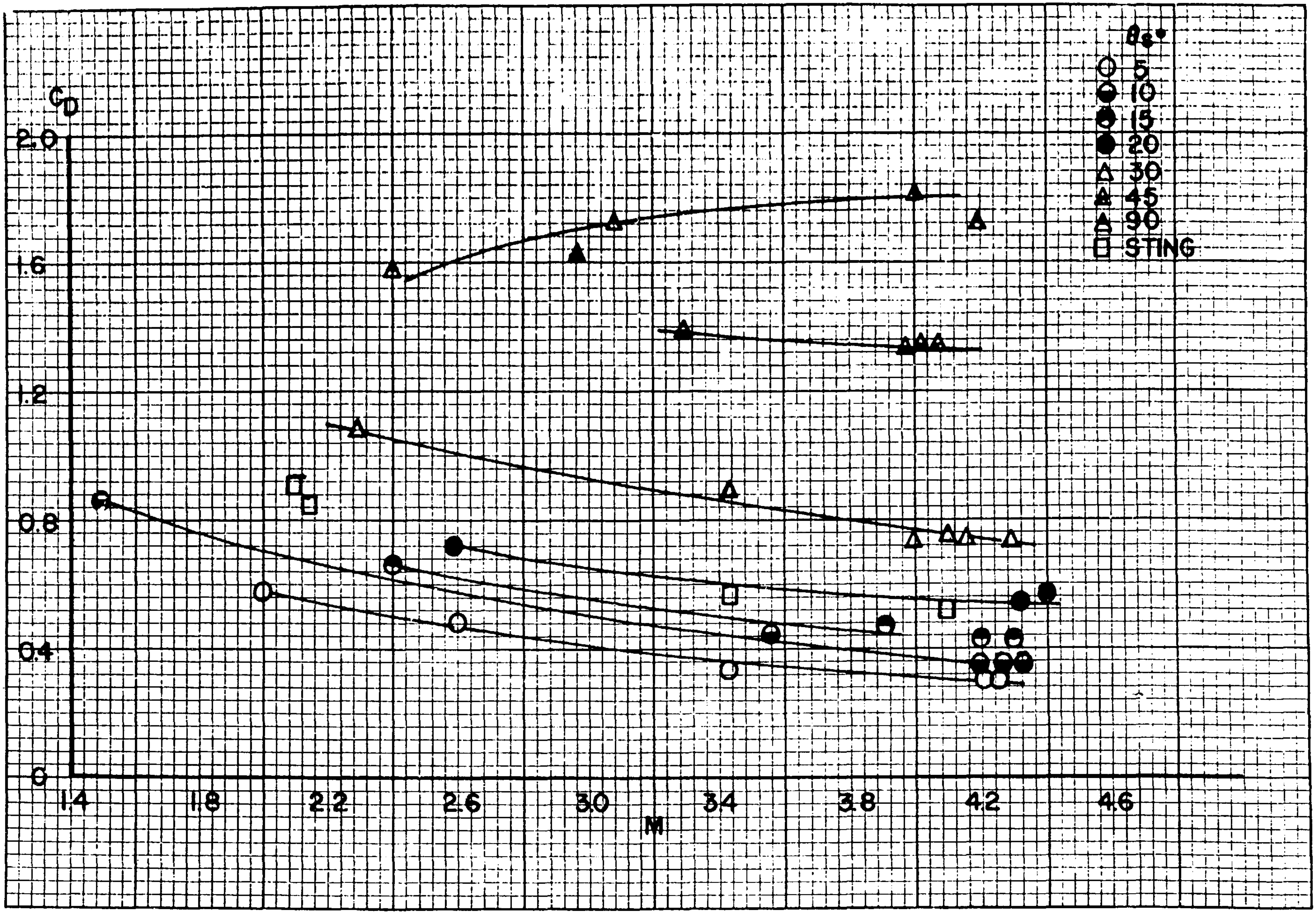

Figure 3. C_D versus Mach Number for Configurations

for small yaw is:

$$C_D = C_{D_o} + C_{D_{\delta^2}} \delta^2$$

In some cases, there were several models of the same type at the same Mach number but with different yaw levels and the C_{D_o} value could be determined directly by plotting the data as a function of yaw level. In cases where this was not possible, $C_{D_{\delta^2}}$ was assumed to be adequately represented by C_{N_α} of the fins and a computed $C_{D_{\delta^2}}$ for the body, for the purpose of the small correction. The curves for the lower values of θ_s exhibit a typical supersonic behavior for a fin stabilized dart and the drag increases are modest until the semi-angle exceeds 15°. The drag increases rapidly for higher semi-angles and the blunt flechette exhibits the continuously increasing drag curve of a blunt body. The data above a Mach number of 3.5 were adjusted to a Mach number of 4.2 and the result plotted as a function of cone angle in Figure 4. This shows the nature of the variation more clearly, the data can be quite closely represented by a $(1 - \cos \theta_s)$ variation up to $\theta_s = 45^\circ$.

<u>Static Moment</u>. The static moment slope C_{M_α} is a function of the center of mass position of the model, and for the test projectiles this is the center of volume; hence, the indicated variation is strictly valid only for the particular parametric family tested. The values of C_{M_α} from the tests are plotted in Figure 5a-b as a function of Mach number. The data were also plotted as a function of yaw in an effort to determine the nature of any variation with yaw. There were not adequate data to establish a reliable correction factor for any type and the variations do not appear to be large. There is a distinct trend in

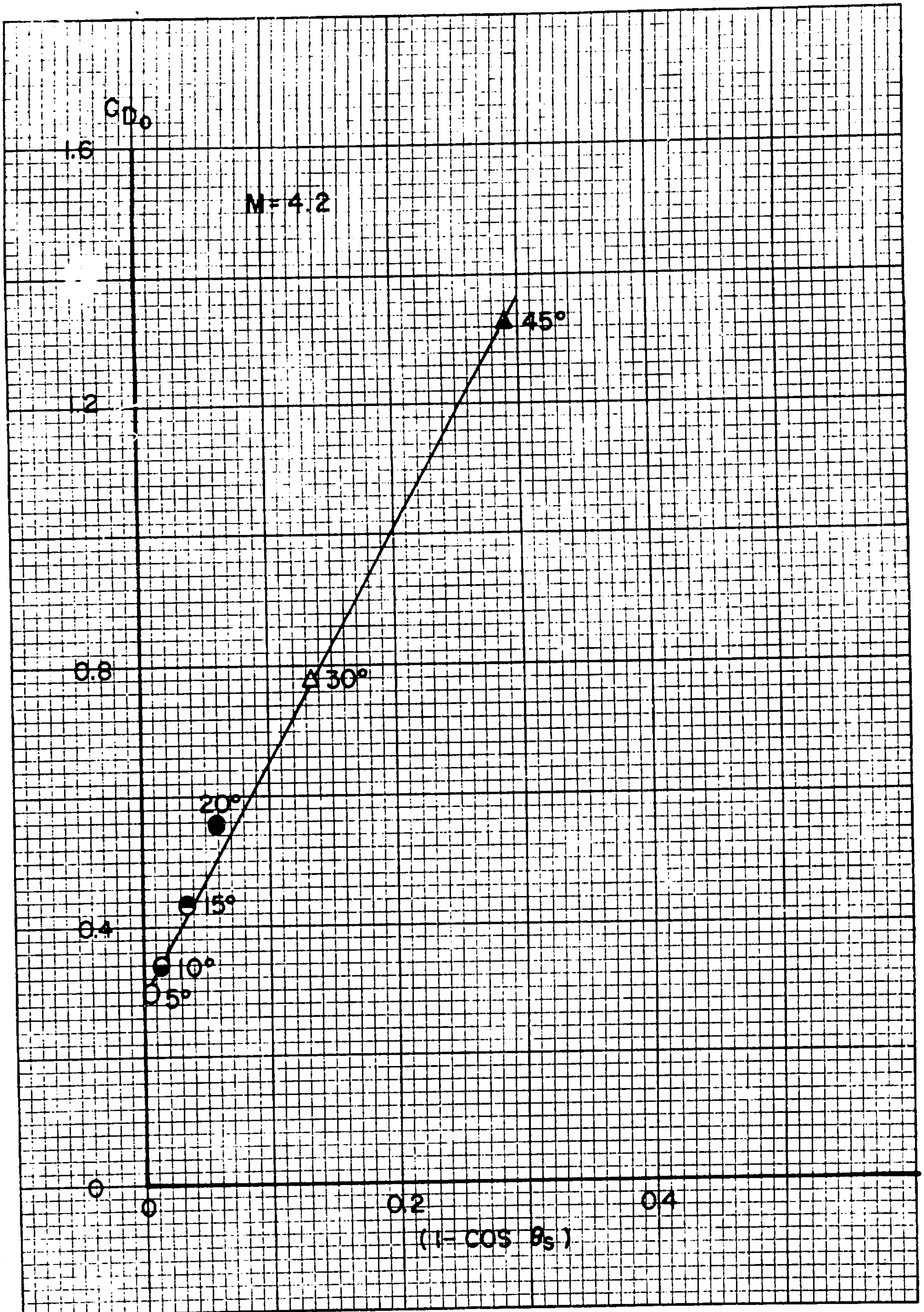

Figure 4. C_D as a Function of Nose Semi-Angle

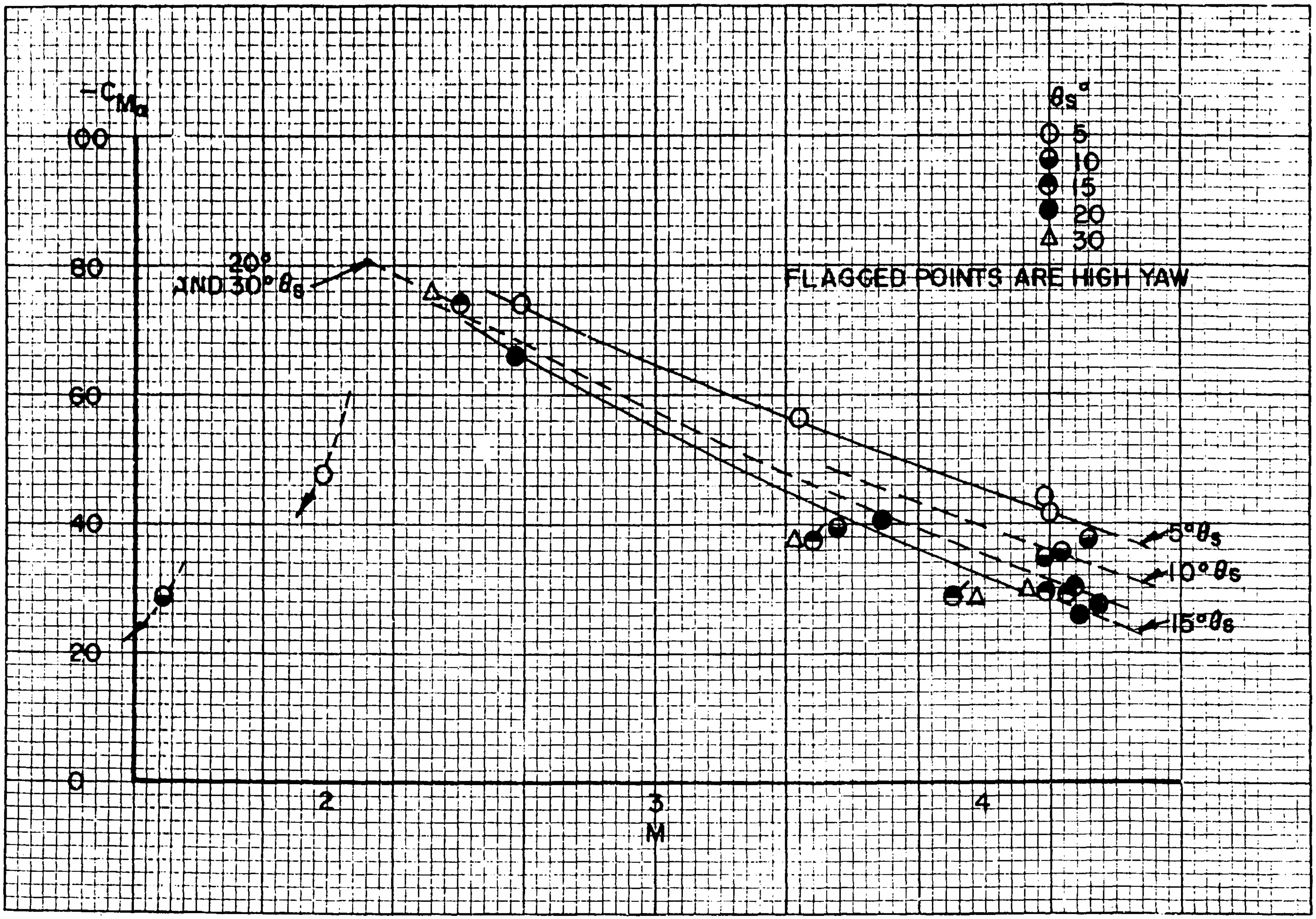

Figure 5a. Static Moment Slope for Configurations

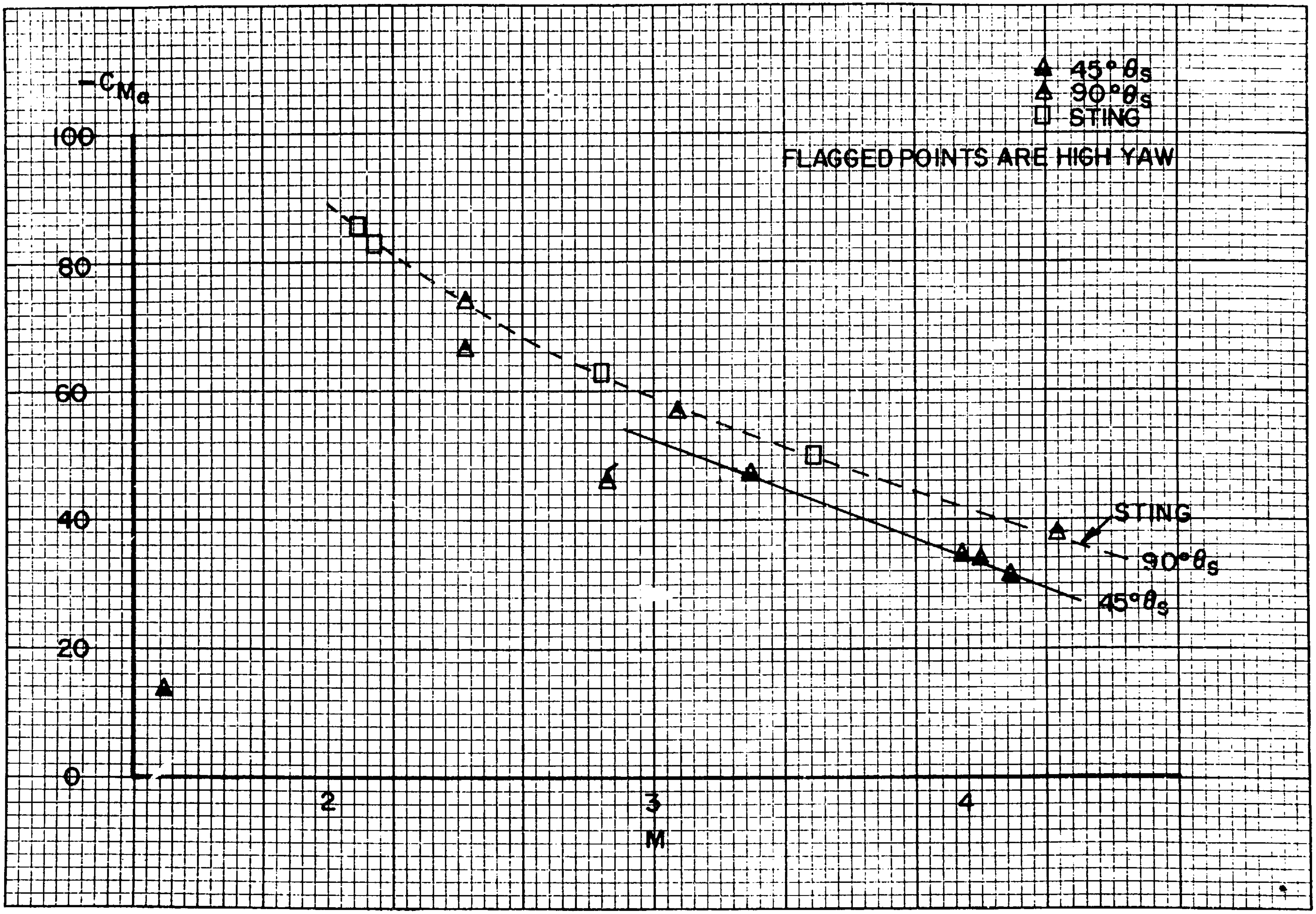

Figure 5b. Static Moment Slope for Configurations

that the values of C_{M_α} for rounds with yaws above about three degrees are significantly smaller in magnitude than those for rounds with two to three degrees of yaw. The rounds with the smallest yaw levels also seem to have smaller values, but this variation is not clearly beyond the data scatter.

The general uniformity of the data as a function of Mach number is somewhat surprising; the variation with Mach number is almost linear for all types from just above Mach 2 to beyond Mach 4 and a bandwidth of about ten units in C_{M_α} would encompass almost all of the smaller yaw data. In fact, only the blunt projectiles and the most pointed ones ($\theta_s = 5^\circ$) appear to have a trend that is distinguishable from the general mass of data and both of these have a greater negative slope by eight to ten units. There are only three data points between Mach 1.5 and 2 and these represent two of the more pointed projectiles and one blunt version; all indicate that the static moment slope is becoming much smaller in magnitude below Mach 2. The stability level decreases with increasing Mach number from Mach 2 up, as is characteristic of fin stabilized projectiles. Extrapolation of the present data would indicate that most of the types would become unstable between about Mach 5.5 and 6; such a linear extrapolation is not really valid and was done only to indicate a probable upper bound for the utility of this particular family.

Normal Force Slope. The normal force slope values are given in Figure 6. In the cases of the drag and static moment, the raw data served a purpose in defining the types but this is not the case for the fewer data on C_{N_α}. The direct data indicate only that all the cases except the 45° and 90° θ_s cases are similar. The latter two cases lie

about 40% below the other data. The C_{N_α} curves in Figure 6 are derived from the stripped-out tail moment results by assuming the tail center of pressure position. One can only say that the direct data generally agree. The more pointed models show a trend from a C_{N_α} of 15 at Mach 2 down to about 11 at Mach 4. The 45° θ_s model shows values perhaps a little more than half as large while the blunt model seems to have even slightly lower values that show little changes with Mach number. The direct and indirect indications for $M \leq 2$ are that there is a decrease in C_{N_α} from that of the $M \doteq 2$ level.

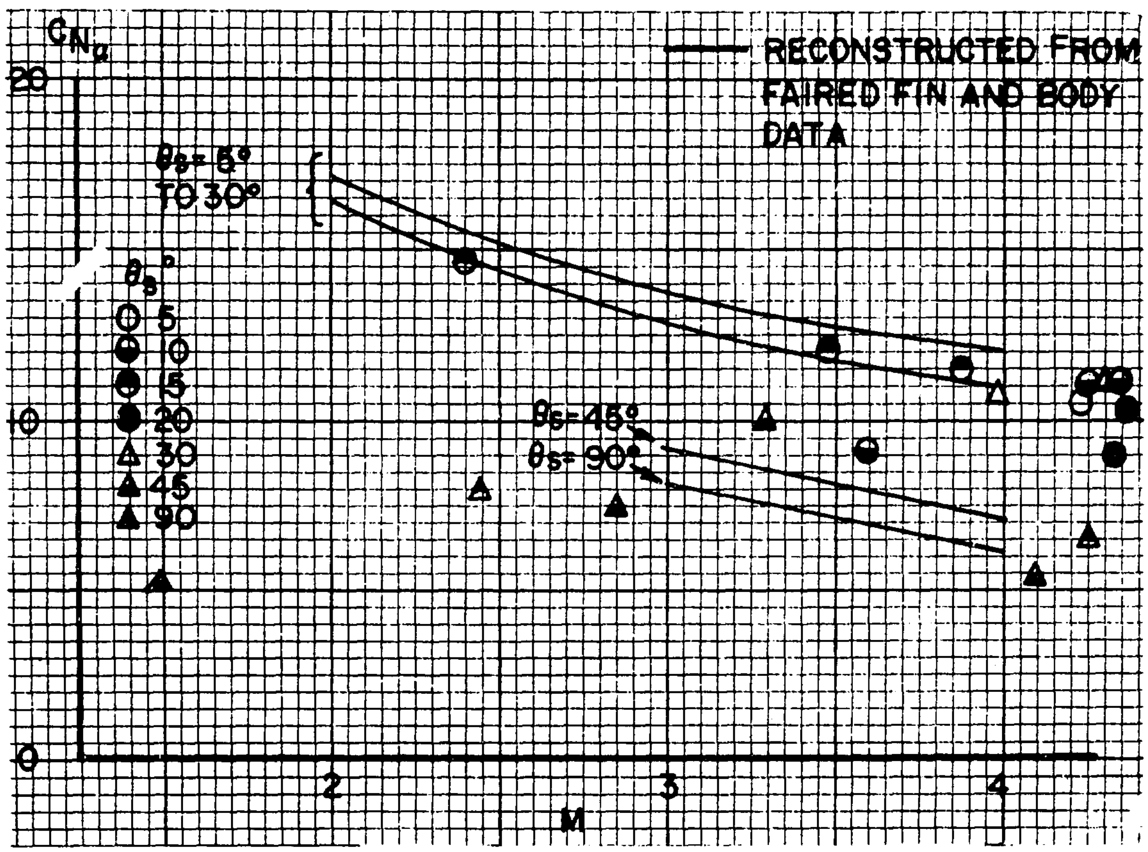

Figure 6. Normal Force Slope for Configurations

Damping Moment Coefficient. The better values of the damping moment derivatives ($C_{M_q} + C_{M_{\dot{\alpha}}}$) are given in Figure 7. There is a general trend from a level of ($C_{M_q} + C_{M_{\dot{\alpha}}}$) = -1400 at Mach 2 to -700 at Mach 4 with no clear definition between types.

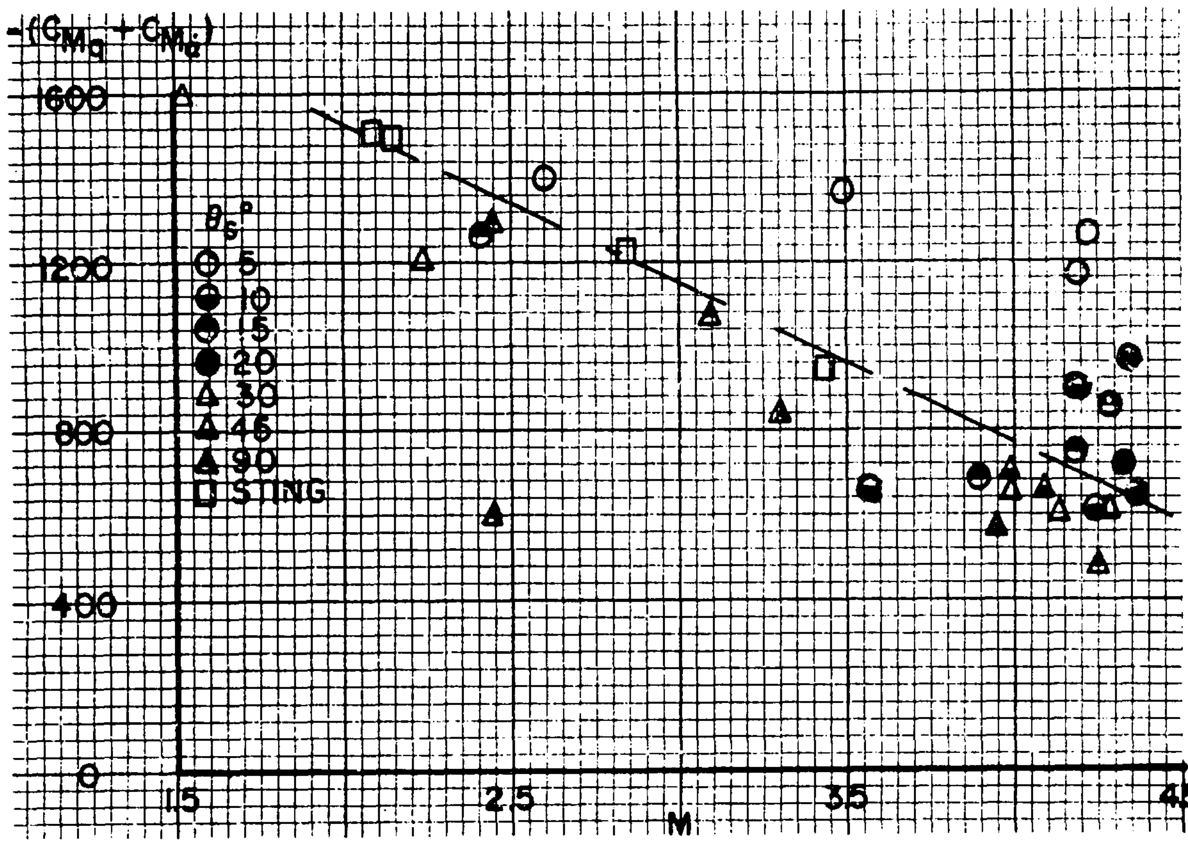

Figure 7. Damping Moment Slopes for Configurations

2. Component Properties

Drag. The drag elements for the various types are given in Figures 8a-g. The drag difference ascribed to the fins is four times the body pressure drag and laminar friction drag for the 5° semi-angle body at Mach 4. In effect, however, all the base drag is being assigned to the fins by this method. The base drag component for the body

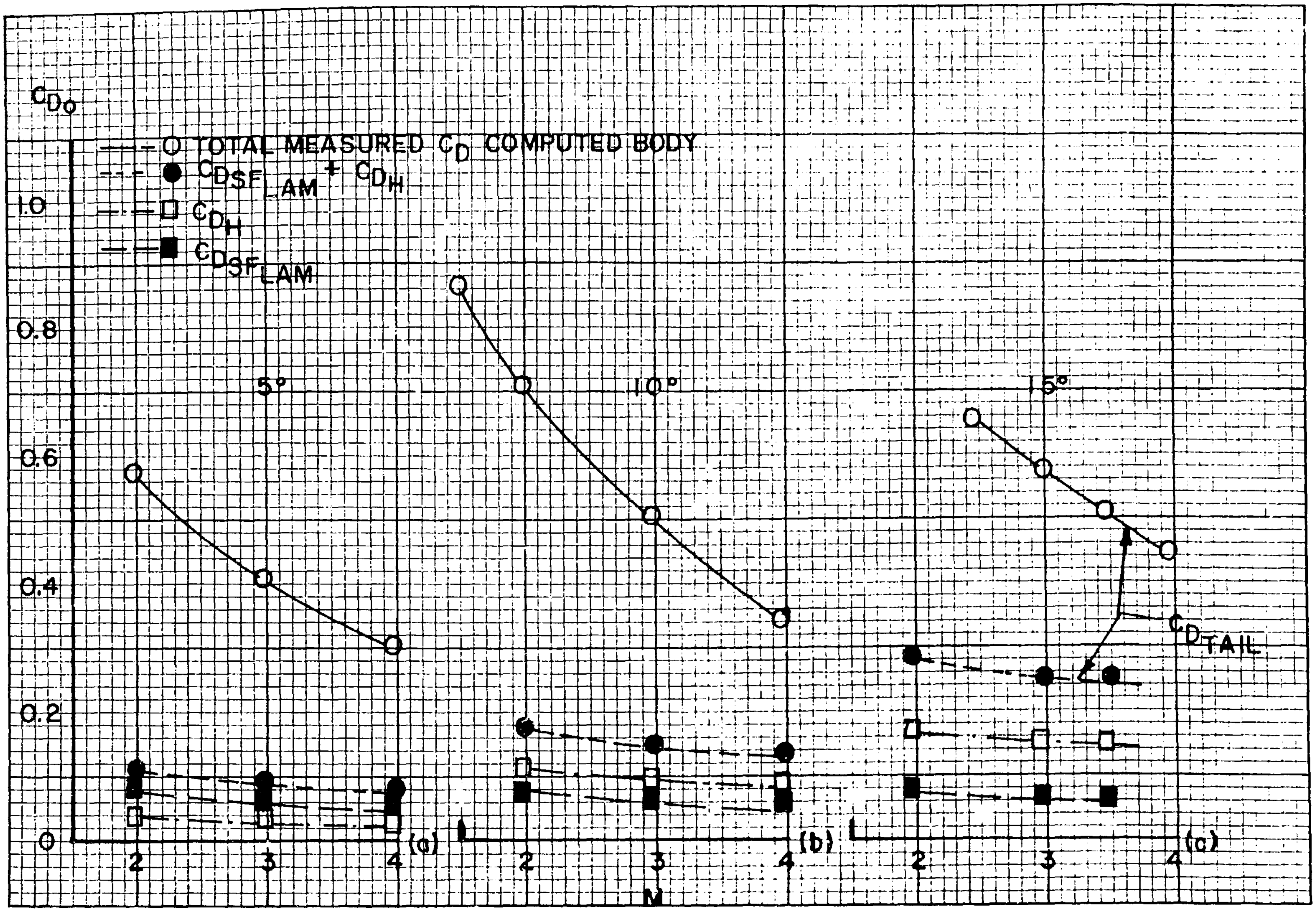

Figure 8. Component Drag Coefficients

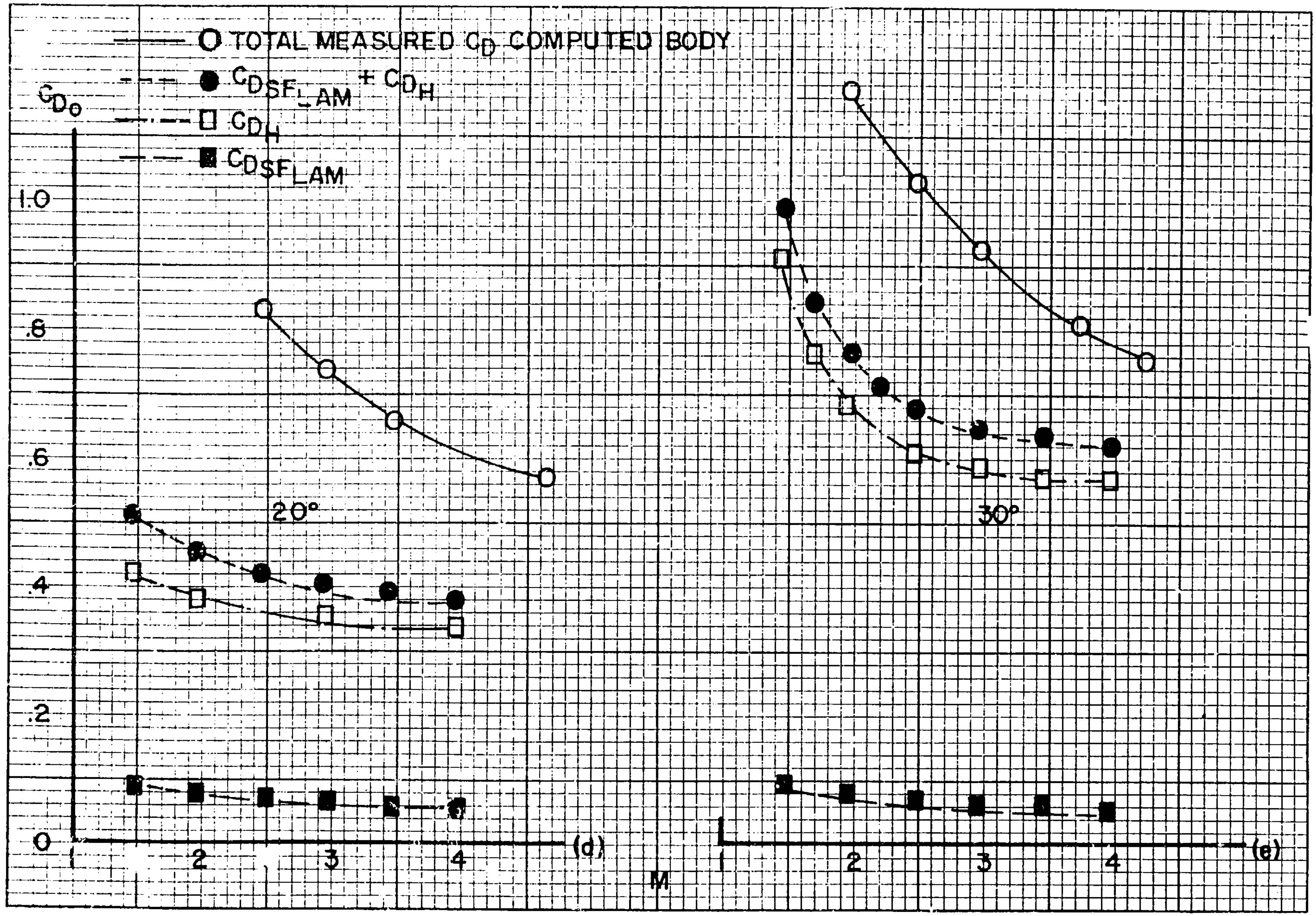

Figure 8. Component Drag Coefficients (Continued)

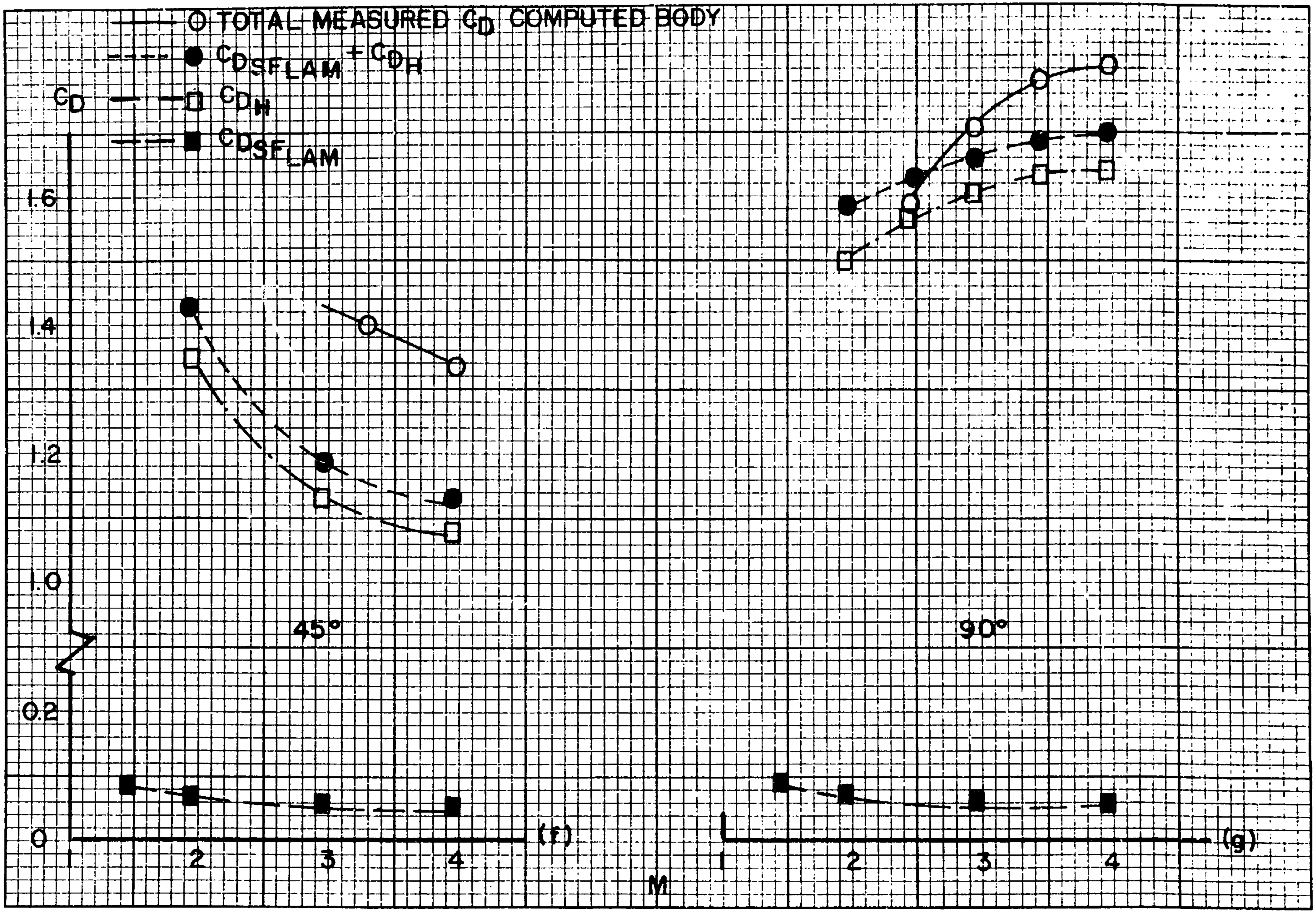

Figure 8. Component Drag Coefficients (Continued)

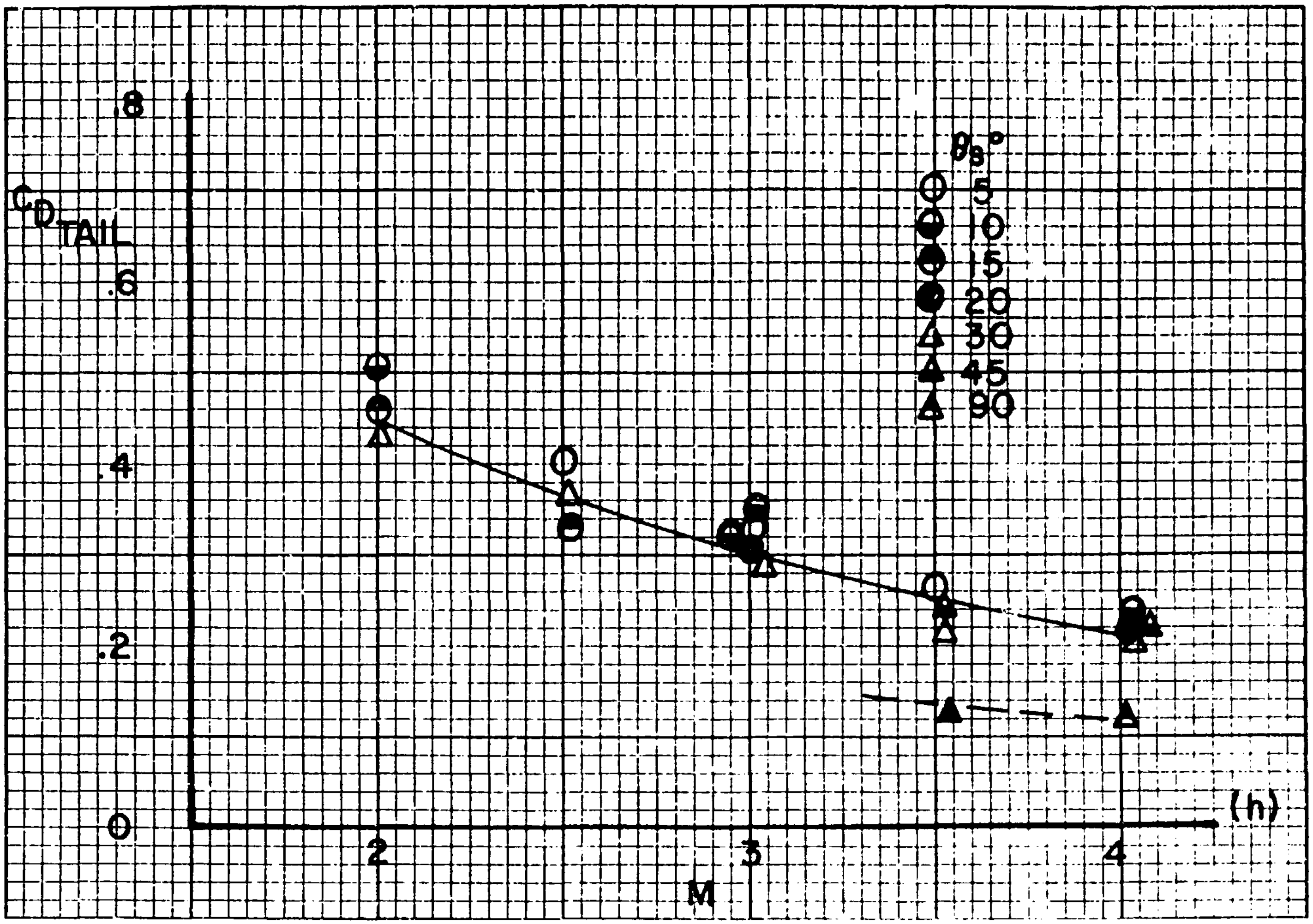

Figure 8. Component Drag Coefficients (Continued)

without fins is larger than the other elements. Including the base drag of the body in the ratio the total measured drag coefficient for the body with fins is only about 50% higher than the computed total drag of the finless body. As the nose becomes blunter, the relative proportions of the elements change slowly until the cone semi-angle exceeds 15° and then rapidly until the tail section drag becomes a small portion of the total drag for $\theta_s > 30^{\circ}$.

The difference between a laminar or turbulent flow over the body is about 0.1 in C_D so that for the more pointed bodies the existence of a turbulent boundary layer, or a cruder fin section, could result in relatively large drag increases. Conversely, for the blunter projectiles, cruder tail assemblies or turbulent flow are less critical to the total drag value.

The result of the subtraction process for total fin section drag coefficient is given in Figure 8h for the conical configurations. The values derived from the various types are consistent to within a total spread of about ± 5% and the differences do not appear systematic. A similar process for the blunt, or 90° θ_s configuration will not yield a consistent value and this is apparent from Figure 8g. However, an error in the estimated body drag of only 6 to 10% would remove this discrepancy and in this particular case such an error is quite probable.

Static Moment. The aerodynamic moment created by the various components is not a basic property since they relate to the particular center of mass position of the total configuration. However, the static moment slope of the total configuration is one of the most accurately determined quantities from a spark range test and thus it serves as a good consistency check and also is one method of estimating the normal force slope of the tail section of this particular

family of flechettes. The computer program used for evaluating the body normal force slope and center of pressure of the 5, 10, and 15° θ_s over the range of Mach number and the 20 and 30° θ_s models at the lower Mach numbers usually agrees with experiment to within about 10%. The more approximate methods used for the other cases with conical heads could have higher errors. The body force estimates for the blunt models, and later for the spiked-nosed model, may be in error by as much as 50% but in these cases the body moment contribution is small.

The body moment, the measured moment and, by summation, the inferred moment coefficient slope of the tail section is presented in Figures 9a-g. In general, the body contribution is small at Mach 2 but by Mach 4 nearly half of the available tail moment is being utilized to overcome the destabilizing body moment for the conical nosed models.

The resultant $C_{M_{\alpha F}}$'s are recollected in Figure 9h. The curve for the 5° θ_s model is above the rest and in general the curves for the various types are distinct. This, however, is primarily the influence of the different moment arms of the configurations. By assuming a center of pressure of the tail assembly, the moment coefficient can be reduced to a tail assembly force coefficient as is done in the next section.

Normal Force Slope. The center of pressure of low aspect ratio supersonic fins is usually near the center of area and this assumption was made to reduce the moment data. The result is the normal force slope of the fin section and this is plotted in Figure 10. Type identification essentially disappears except that the 45° θ_s and the blunt model show lower values. This may be due to dynamic pressure losses in the local flow caused by the blunter noses.

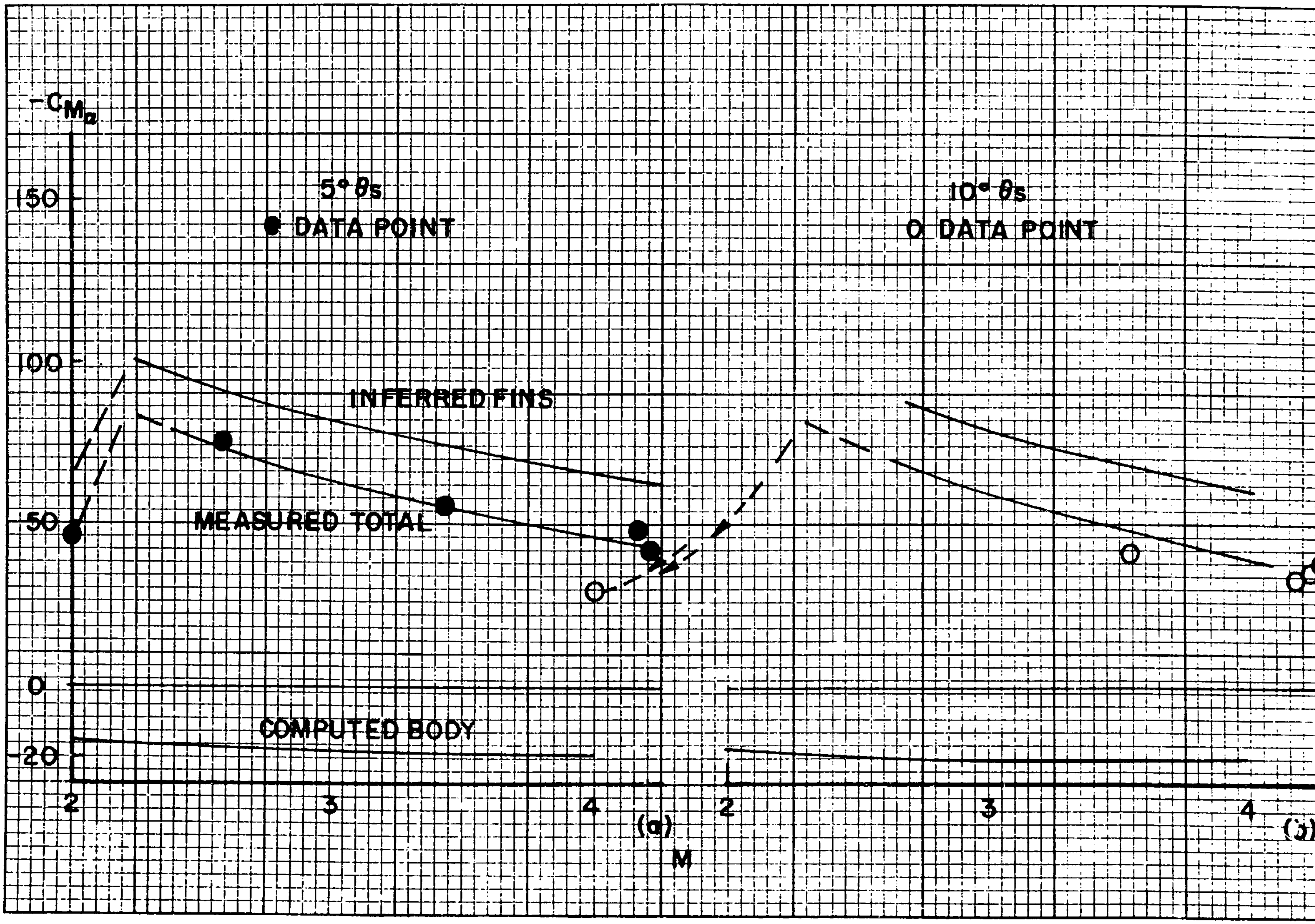

Figure 9. Static Moment Slope Components

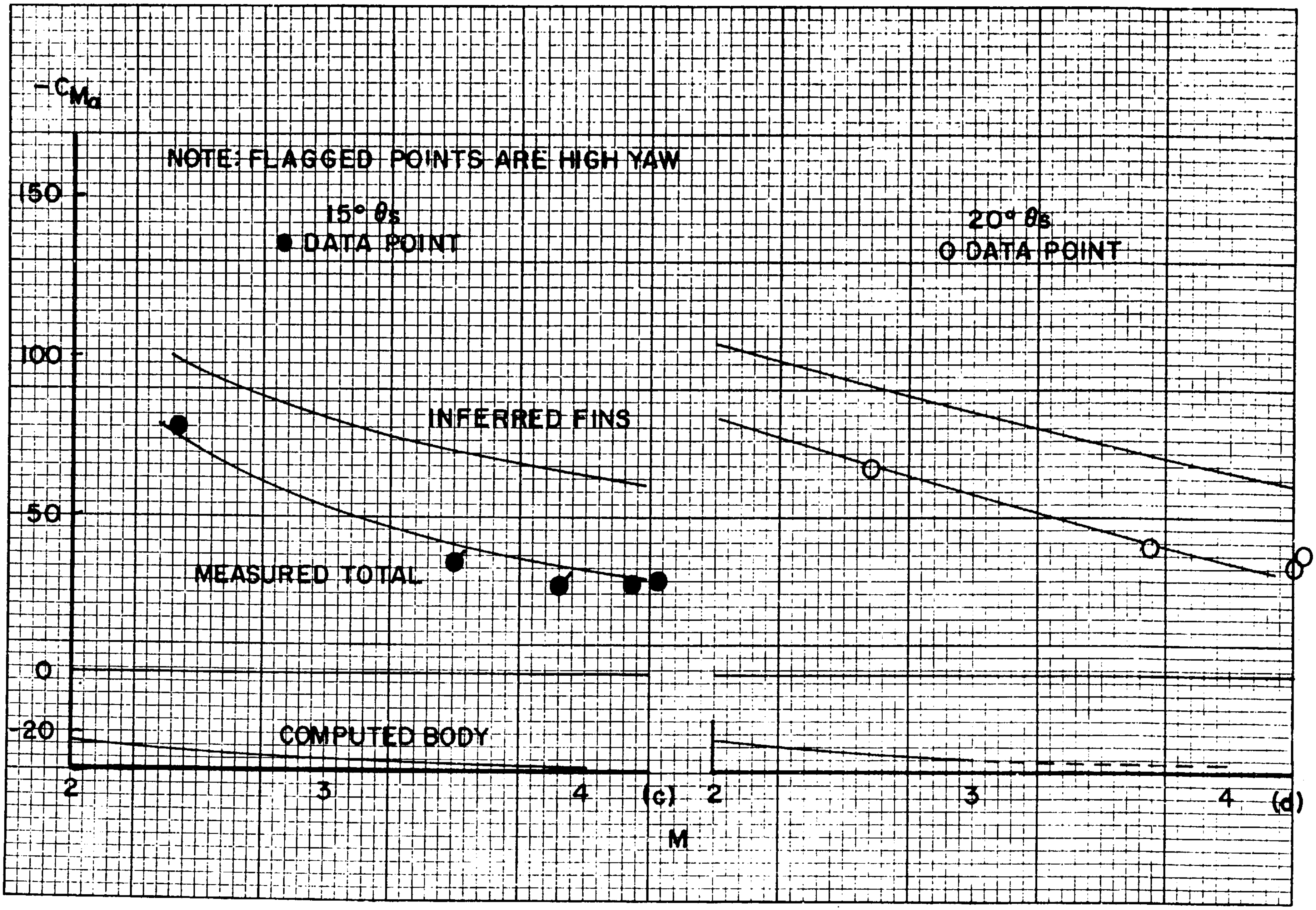

Figure 9. Static Moment Slope Components (Continued)

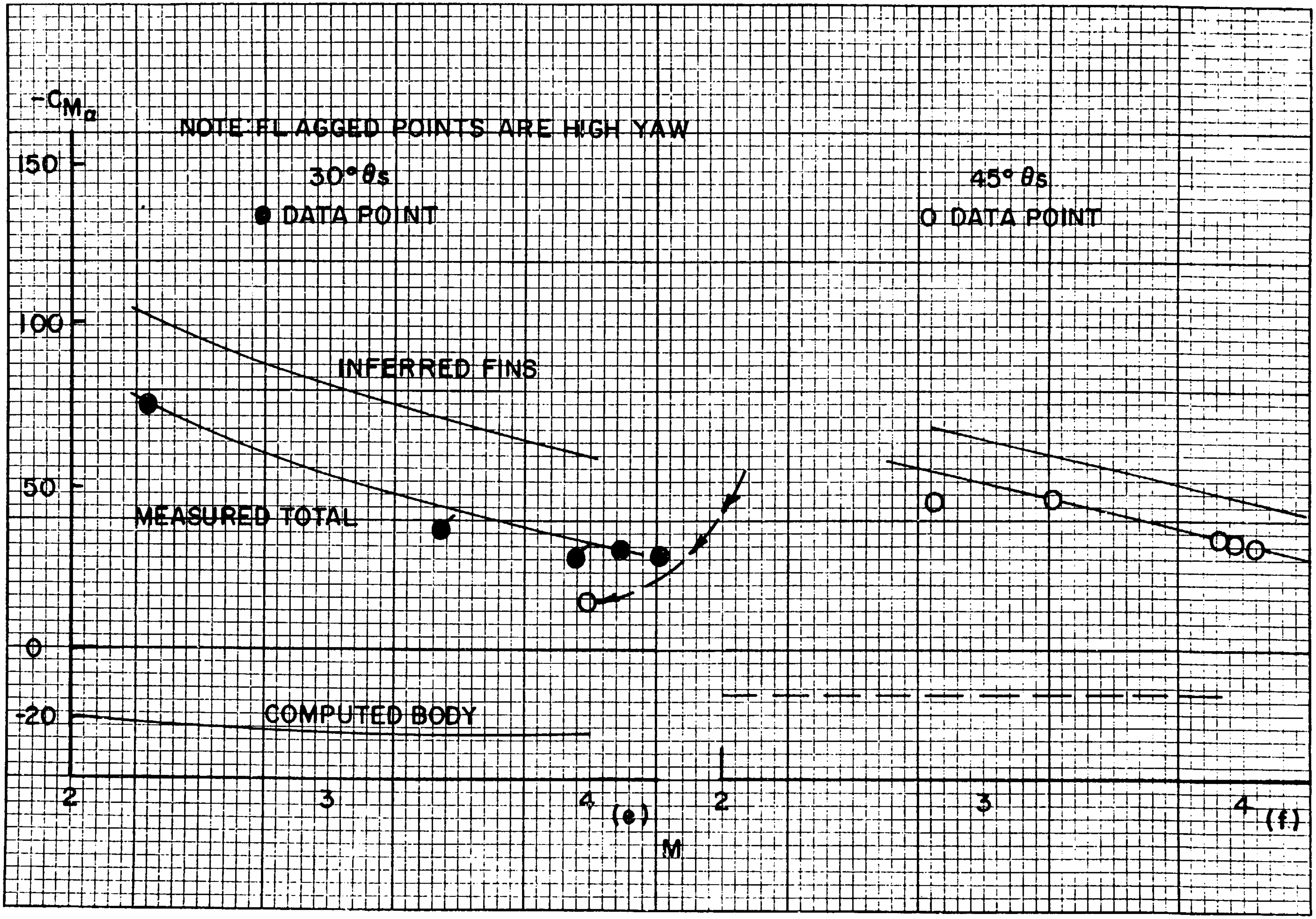

Figure 9. Static Moment Slope Components (Continued)

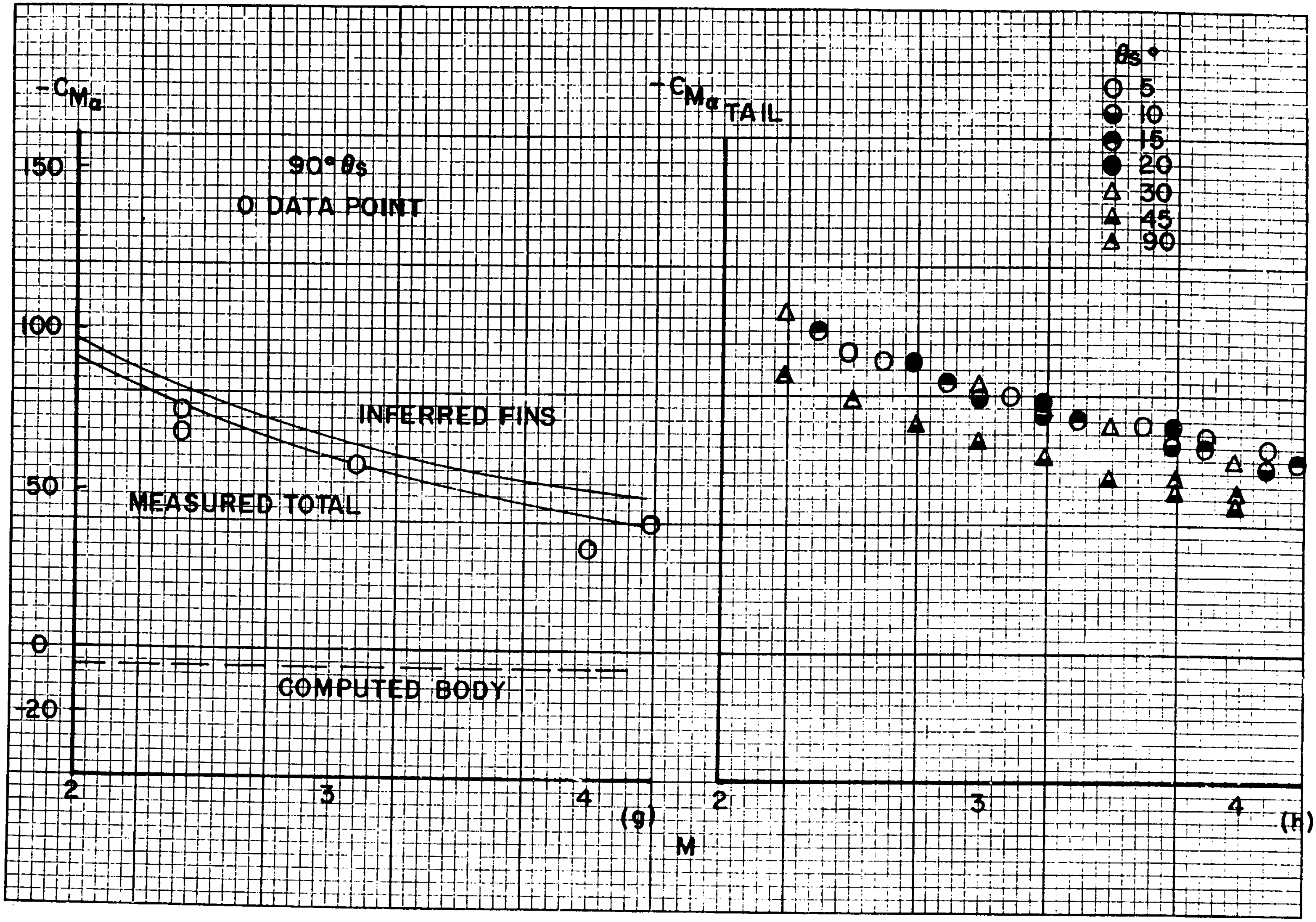

Figure 9. Fin Assembly Static Moment Slope

The fin C_{N_α} may also be obtained by subtracting the body C_{N_α} from the measured C_{N_α} for the configuration. This, again, results in assigning all the interference effects to the fin assembly. These data are also plotted in Figure 10.

The few values below Mach 2 are at a lower level and in part this should be true because of a change in flow pattern. A swept fin undergoes a loss of lift when the fin leading edge lies behind the apex shock wave. Although the existing fins are stamped and a curved ogee plan form results, the plan form can be enclosed by a tri-angular fin that would have subsonic leading edges at Mach 2 and below. Figure 2i is a shadowgraph of one of the projectiles at Mach 1 and the fin leading edge is clearly behind the shock. The indicated loss is larger than would be predicted by linear theory for a tri-angular fin alone. This may be due to body-fin interference effects or, more probably, represents the fact that the sharpened, flat, fins are efficient supersonic airfoils but are poorer subsonic sections.

3. Spike-Nosed Projectile

It was of interest to check the feasibility of using spike-nosed projectiles in flechette sizes. On larger shell, the spike reduces the drag level while retaining the high stability properties of the fin stabilized flat nosed projectile. The price of the improvement offered by the spike depends on the nature of the flow separation area formed by the spike[5]. On larger projectiles, trip devices can be used to control the flow. On a very small projectile, it is not clear that the spike alone is mechanically practical and trip mechanisms affixed to the tiny spike certainly would not be. In the case of larger projectiles, the flow before separation is usually turbulent while the boundary layer on the flechette is laminar.

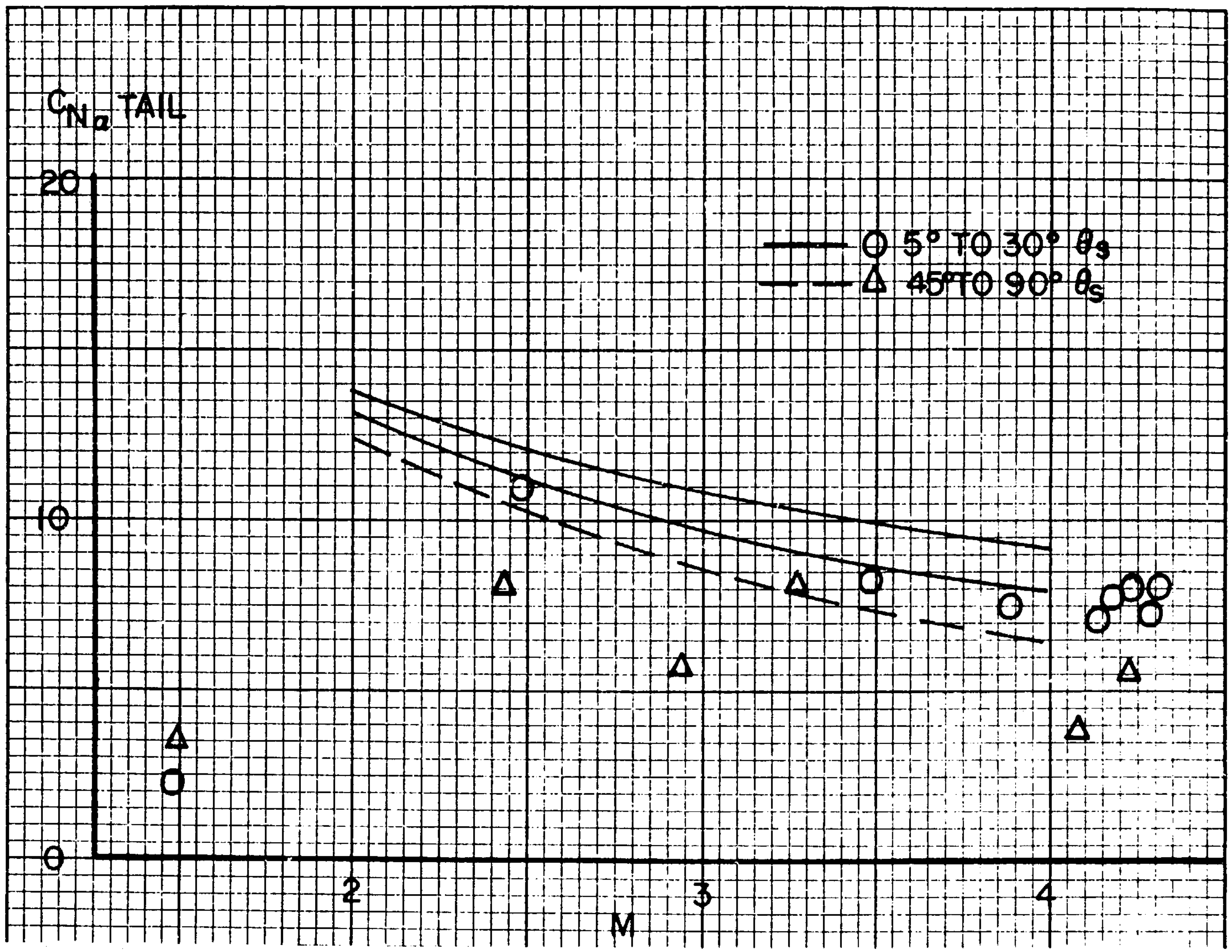

Figure 10. Fin Assembly Normal Force Slope

In order to obtain an indication of possible performance a few spike-nosed flechettes were manufactured, and a few of these were launched successfully. A sketch of the projectile and an inflight shadowgraph are given in Figures 1 and 2h.

The spike did produce a lower drag value than the blunter conical nose. The drag coefficient was comparable with that of the 15° θ_s model and the data are shown with this curve in Figure 11a. Separation was not maintained over the full length of the sting and the length of the separated region approximated the head length of the 15° conical nose. If the separation region could be lengthened by trip devices the drag could be further reduced. The moment coefficient and the normal force coefficients for the spike-nosed models are shown in Figures 11b and 11c. The model has a relatively high moment and a low normal force compared with the conical models of comparable drag. As a result, the sensitivity of the projectile to launch disturbance should be lower. The damping moment slopes are given in Figure 11d.

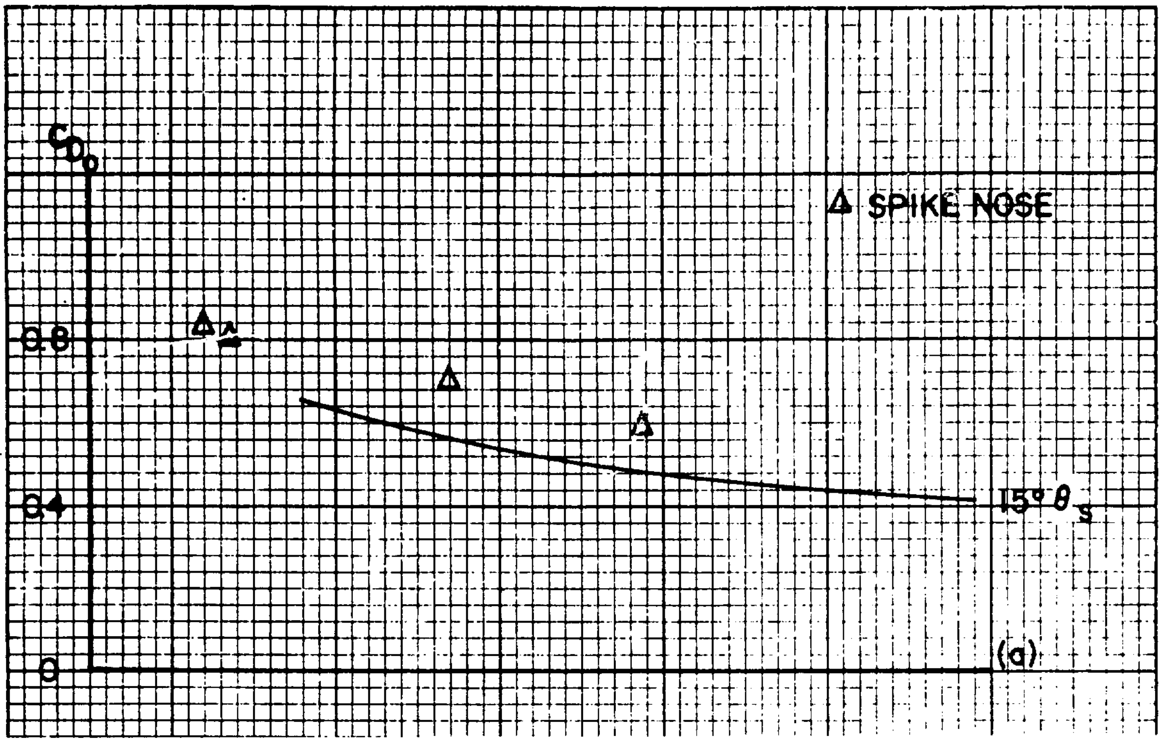

Figure 11a. Drag Coefficient of Spike-Nosed Configuration

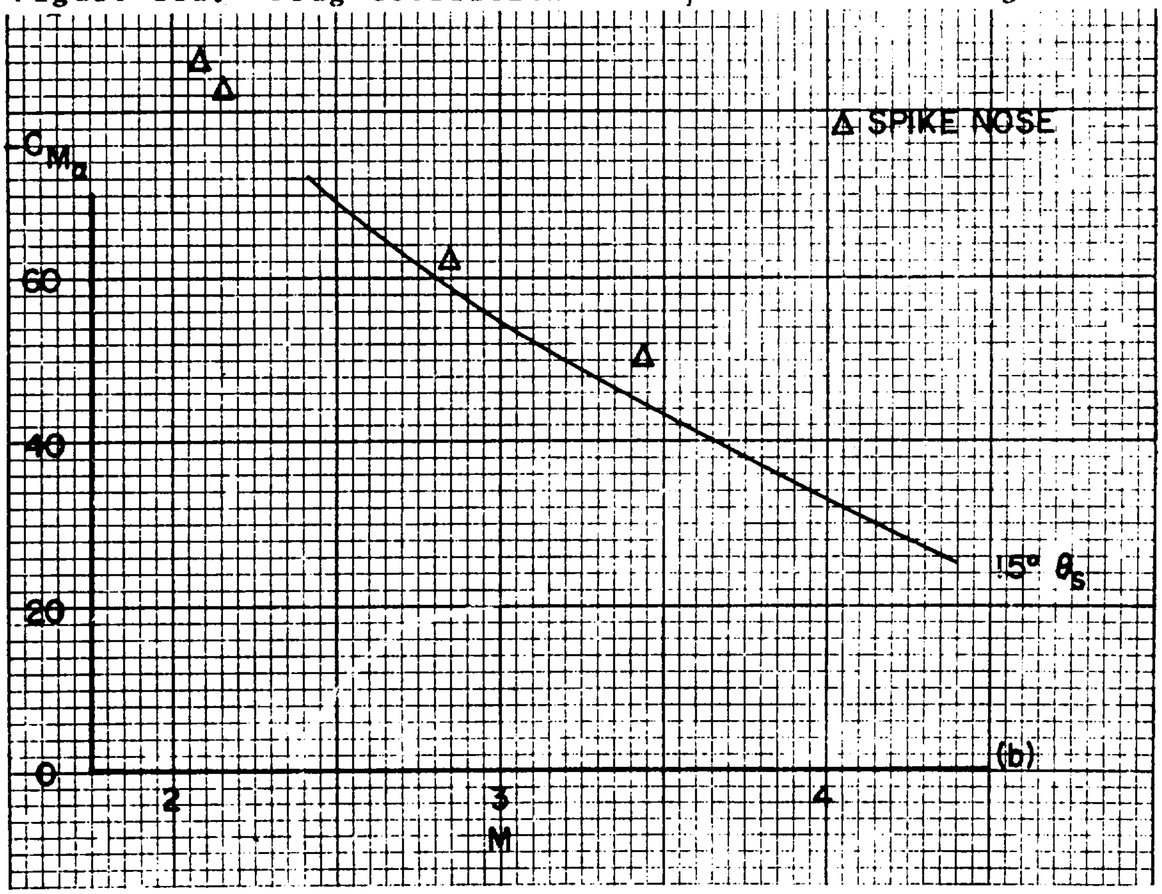

Figure 11b. Static Moment Slope of Spike-Nosed Configuration

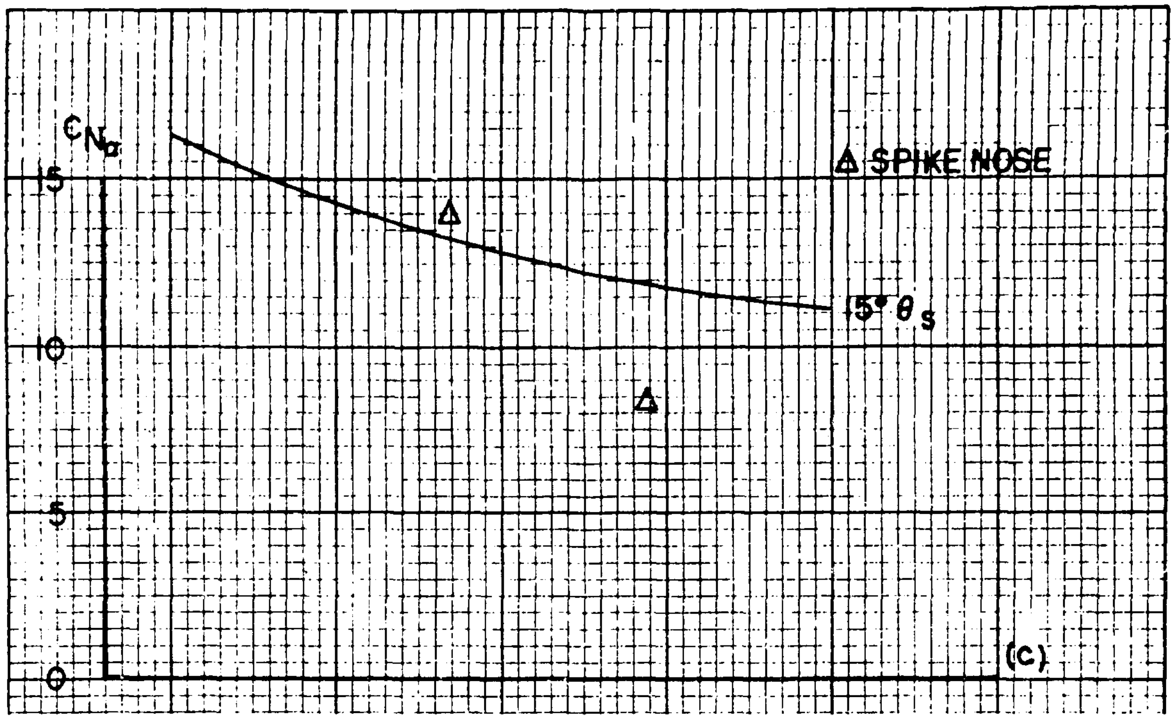

Figure 11c. Normal Force Slope of Spike-Nosed Configuration

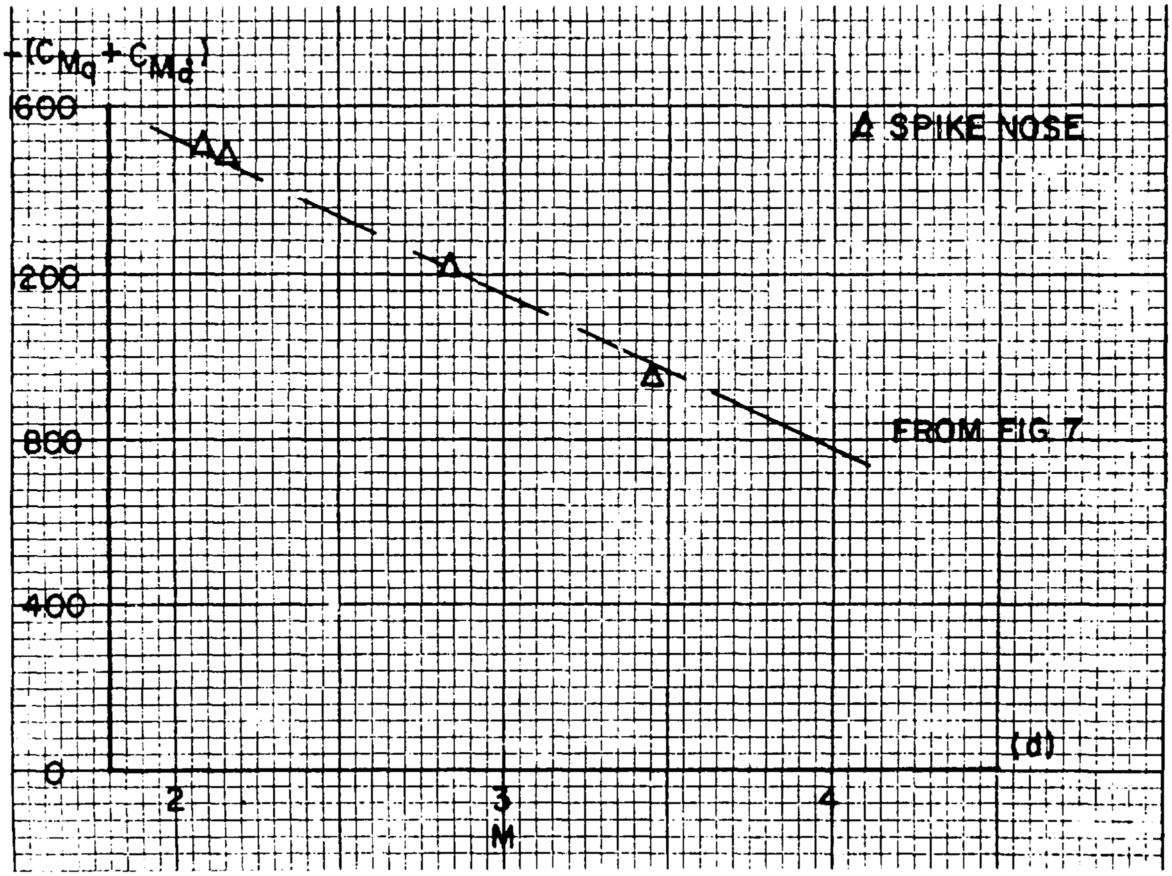

Figure 11d. Damping Moment Slope of Spike-Nosed Configuration

REFERENCES

1. Maynard J. Piddington, "The Aerodynamic Characteristics of A S.P.I.W. Projectile", Ballistic Research Laboratories Memorandum Report 1594, September 1964, (AD 355679).

2. Walter F. Braun, "The Free Flight Aerodynamics Range", Ballistic Research Laboratories Report 1048, July 1958, (AD 202249).

3. Charles H. Murphy, "Data Reduction for the Free Flight Spark Ranges", Ballistic Research Laboratories Report 900, February 1954, (AD 35833).

4. M. D. VanDyke, "First and Second Order Theory of Supersonic Flow Past Bodies of Revolution", Journal of the Aeronautical Sciences, March 1951.

5. Branimir D. Djordjevic, "Aerodynamic Force Analysis", Vol. II, Department of Aerospace Engineering, Auburn University, Contract DA-01-009-506-ORD-8511Z), June 1966, (AD 802294).

6. Boris G. Karpov and Maynard J. Piddington, "Effect on Drag of Two Stable Flow Configurations over the Nose of the 90mm T316 Projectile", Ballistic Research Laboratories Technical Note 955, October 1954, (AD 479828).

Unclassified
Security Classification

DOCUMENT CONTROL DATA - R & D

(Security classification of title, body of abstract and indexing annotation must be entered when the overall report is classified)

1. ORIGINATING ACTIVITY (Corporate author) U.S. Army Aberdeen Research & Development Center Ballistic Research Laboratories Aberdeen Proving Ground, Maryland	2a. REPORT SECURITY CLASSIFICATION Unclassified 2b. GROUP NA

3. REPORT TITLE

Drag and Stability Properties of the XM144 Flechette with Various Head Shapes

4. DESCRIPTIVE NOTES (Type of report and inclusive dates)

BRL Memorandum Report

5. AUTHOR(S) (First name, middle initial, last name)

Leonard C. MacAllister

6. REPORT DATE	7a. TOTAL NO. OF PAGES	7b. NO. OF REFS
May 1969	46	6

8a. CONTRACT OR GRANT NO. b. PROJECT NO. RDT&E 1T262301A201 c. d.	9a. ORIGINATOR'S REPORT NUMBER(S) Memorandum Report No. 1981 9b. OTHER REPORT NO(S) (Any other numbers that may be assigned this report)

10. DISTRIBUTION STATEMENT

This document is subject to special export controls and each transmittal to foreign governments or foreign nationals may be made only with prior approval of Commanding Officer, U.S. Army Aberdeen Research and Development Center, Aberdeen Proving Ground, Maryland.

11. SUPPLEMENTARY NOTES	12. SPONSORING MILITARY ACTIVITY
	U.S. Army Materiel Command Washington, D.C.

13. ABSTRACT

The drag and stability properties of a family of flechettes with conical heads are presented; cone semi-angles varied from 5 to 90 degrees. The data cover a range from Mach 2 to Mach 4 and were determined from free flight spark range tests. Limited results on a spike-nosed configuration are also given. ( )

DD FORM 1 NOV 65 1473 REPLACES DD FORM 1473, 1 JAN 64, WHICH IS OBSOLETE FOR ARMY USE.

Unclassified
Security Classification

14. KEY WORDS	LINK A		LINK B		LINK C	
	ROLE	WT	ROLE	WT	ROLE	WT
Aerodynamics Ordnance Flechettes						